On the Increased Frequency of Mediterranean Drought

Martin Hoerling, Jon Eischeid, Judith Perlwitz, XiaoWei Quan,
Tao Zhang, Philip Pegion

NOAA Earth System Research Laboratory, Boulder Colorado USA

Revised Manuscript Submitted to

Journal of Climate

2 September 2011

ABSTRACT

The land area surrounding the Mediterranean Sea has experienced ten of the twelve driest winters since 1902 in just the last 20 years. A change in wintertime Mediterranean precipitation toward drier conditions has likely occurred over 1902-2010 whose magnitude cannot be reconciled with internal variability alone. Anthropogenic greenhouse gas and aerosol forcing are key attributable factors for this increased drying, though the external signal explains only half of the drying magnitude. Furthermore, sea surface temperature (SST) forcing during 1902-2010 likely played an important role in the observed Mediterranean drying, and the externally forced drying signal likely also occurs through an SST change signal.

The observed wintertime Mediterranean drying over the last century can be understood in a simple framework of the region's sensitivity to a uniform global ocean warming and to modest changes in the ocean's zonal and meridional SST gradients. Climate models subjected to a uniform +0.5°C warming of the world oceans induce eastern Mediterranean drying, but fail to generate the observed wide-spread Mediterranean drying pattern. For a +0.5°C SST warming confined to tropical latitudes only, a dry signal spanning the entire Mediterranean region occurs. The simulated Mediterranean drying intensifies further when the Indian Ocean is warmed +0.5°C more than the remaining tropical oceans, an enhanced drying signal attributable to a distinctive atmospheric circulation response resembling the positive phase of the North Atlantic Oscillation. The extent to which these mechanisms and the region's overall drying since 1902 reflect similar

mechanisms operating in association with external radiative forcing are discussed.

115 **1. Introduction**

116 Half of Mediterranean land areas are devoted to agriculture consuming 60% to 80%
117 of water supply (ESPERE 2006). It is in this context that increased drought
118 frequency observed over land areas surrounding the Mediterranean Sea in recent
119 decades (e.g., Mariotti 2010) is of great concern because of the threats posed to the
120 region's food security (IFPRI 2009). The region, which accumulates most of its
121 annual precipitation via migratory storms during November-April, is shown in this
122 paper to have experienced ten of the twelve driest winter seasons since 1902 in just
123 the last 20 years (Fig. 1, top). In concert with this drying trend, which has been a
124 cold season phenomenon to date, precipitation has increased over northern Europe
125 since 1902. The south-north contrast in European precipitation trends over the last
126 century (Fig. 1, bottom) resembles anomaly patterns occurring on interannual and
127 decadal time scales--- often associated with fluctuations of the North Atlantic
128 Oscillation (NAO), the dominant structure of North Atlantic atmospheric variability
129 that is linked to storm track changes over Europe (e.g., Hurrell 1995; Jones et al.
130 2003; Hurrell and Deser 2009; Mariotti and Dell' Aquila 2011). Also, such a south-
131 north contrast in precipitation trends describes the pattern of climate change in
132 projections toward the end of the 21st Century in models forced by scenarios of
133 increasing anthropogenic greenhouse gases conducted as part of the
134 Intergovernmental Panel on Climate Change (IPCC) Fourth Assessment (Ulbrich et
135 al. 2006; Solomon et al, 2007; Mariotti et al. 2008). By the latter decades of the 21st
136 Century, the Mediterranean region is projected to experience the greatest drying (as

137 a percentage of climatological rainfall) among 26 regions across the globe (Giorgi
138 2006).
139
140 The latter acuteness in IPCC model projections of anthropogenic impacts has earned
141 the Mediterranean region the title of major "climate change hot spot" (Giorgi 2006).
142 It is believed that changes in zonal mean atmospheric circulation would become an
143 effective mechanism for inducing a drying of lower mid-latitudes, including the
144 Mediterranean region, in response to increasing greenhouse gas concentrations (e.g.
145 Seager et al. 2007; Seager et al. 2010). Such drying would occur mainly through a
146 poleward shift of subtropical dry zones due to a poleward expansion of the Hadley
147 Cell (e.g., Lu et al. 2007) and a poleward shift of the storm tracks (e.g., Yin 2005;
148 Previdi and Liepert 2007).
149
150 This paper explores possible causes for increased Mediterranean drought observed
151 during recent decades, the results of which contribute to the current understanding
152 of the physical processes exposing the Mediterranean region as one of heightened
153 sensitivity to anthropogenic greenhouse gas forcing. In order to understand the
154 mechanisms associated with recent observed drying, we focus on the
155 responsiveness of the region's wintertime precipitation to patterns of sea surface
156 temperature (SST) forcing that describe principal features of the ocean's change
157 during the last century. Previous studies have shown that global SSTs exert an
158 important controlling effect on North Atlantic/European climate via a sensitivity of
159 the wintertime NAO (e.g., Mehta et al. 2000; Robertson et al. 2000; Hoerling et al.

2001; Sutton et al. 2001); in particular, a trend toward a positive phase of the NAO during 1950-1999 was found to be consistent with an atmospheric response pattern forced by Indian Ocean warming (Bader and Latif 2003; Hurrell et al. 2004; Hoerling et al. 2004; Li et al. 2006). Given the strong external radiative contribution to Indian Ocean warming in recent decades (e.g., Knutson et al. 2006), these studies have advanced a theory that anthropogenic forcing may have already contributed to recent North Atlantic and Mediterranean climate trends. Such a notion appears to be consistent with the subsequent analyses of Mariotti et al. (2008) who document a decline in Mediterranean annual precipitation during the 20th Century in CMIP3 simulations (at the rate of -0.007 *mm/d per decade*), followed by more rapid drying after 2020.

However, there are certain facts that a hypothesis of climate change forcing of Mediterranean wintertime drying has failed to explain. Foremost, whereas most coupled models subjected to 20th Century time varying external radiative forcing yield Indian Ocean warming, there is not a consistent North Atlantic atmospheric circulation response resembling the positive NAO index in those models (e.g. Gillett et al. 2003; Osborn 2011). Here we will demonstrate that it is not the Indian Ocean warming per se to which the NAO is primarily sensitive, but the difference between warming rates of the Indian Ocean and the remainder of the tropical oceans. Furthermore, updated observational time series of NAO indices reveal that a trend toward the positive polarity of the NAO, that was particularly strong when diagnosed for the 1950-1999 period as done in most prior studies, is considerably

183 weaker when using additional data through 2010. The question has been raised,
184 therefore, whether the observed variations in the winter NAO index can be
185 explained as internally generated atmospheric variability alone (Wunsch 1999;
186 Osborn 2011). Indeed, analysis presented herein suggests only a small, statistically
187 insignificant, upward trend of the NAO during 1902-2010 which fails to explain the
188 considerable wintertime drying of the Mediterranean during this period.
189
190 It is also not known whether, or to what extent, the zonal mean circulation has
191 changed since the beginning of the 20th Century, in particular if the relationship
192 between tropical and mid-latitude zones has changed through which increased
193 Mediterranean drought might emerge. Davis and Rosenlof (2011) illustrate the
194 sensitivity of recent trends in the width of the tropical belt to the use of various
195 subjective definitions such as the tropopause height or a threshold value of outgoing
196 longwave radiation. For one particular indicator of the width of the tropical belt,
197 namely the Hadley cell extent, they find a statistically significant poleward
198 expansion in three of four reanalysis products for the period 1979-2009. Other
199 indicators of the width of the tropics, including ones based on observations, do not
200 show significant change. For instance, there has been no detected change in the
201 zonal averages of land precipitation during 1925-1999 within the extratropical band
202 30°N-50°N (Zhang et al. 2007), though this may result from the cancellation of
203 strong regional signals of precipitation change that have opposite signs.
204
205 In the current study, we employ global methods involving climate models subjected

206 to external radiative and surface boundary forcings in order to understand drought
207 spanning the region that includes all Mediterranean land areas. Section 2 describes
208 the observational data sets and model simulations, many of which have been used in
209 prior climate studies. New suites of atmospheric model simulations are also
210 conducted that use idealized patterns of SST anomalies. These, also described in
211 section 2, facilitate reconciliation between observed increases in drought frequency,
212 the sensitivity to external radiative forcing, and the role of ocean conditions and
213 atmospheric circulation patterns.
214
215 Results are given in section 3, where we present evidence that a change in the
216 region's climate has been detected, and that it is unlikely that the observed
217 November-April Mediterranean drying since 1902 occurred due to internal
218 variability alone. Diagnosis of the CMIP3 coupled models reveals that this detected
219 change toward drier conditions is attributable, in part, to the Mediterranean
220 region's sensitivity to time evolving external radiative forcing. The amplitude of the
221 externally forced, area-averaged drying signal is roughly ½ the magnitude of the
222 observed drying during 1902-2010, indicating that other processes likely also
223 contributed. Section 3 presents analyses of atmospheric GCM simulations forced
224 with observed SST and sea ice variability since 1902 but using fixed external
225 radiative forcing (so-called AMIP simulations). These reveal that SST forcing was
226 likely an important factor in the observed drying, and furthermore that the
227 externally forced drying signal likely also occurs through an impact of an SST
228 change. Section 4 explores the sensitivity of Mediterranean climate to idealized

patterns of SST forcing that depict gross global features of the CMIP3 and observed patterns of SST change since 1902. It is found that a globally uniform +0.5°C warming of the world oceans produces drying over the eastern Mediterranean, but fails to produce widespread drying over all Mediterranean land areas. A larger amplitude and more expansive drying that includes all Mediterranean land areas emerges when tropical SST warming is greater than extratropical SST warming (a meridional gradient). The magnitude of drying increases yet further in the presence of an ocean condition in which the tropical Indian Ocean SSTs are warmed more than the rest of the tropical oceans (a zonal gradient). These rainfall sensitivities are explained in the context of atmospheric circulation responses to the SST forcing scenarios. Summary comments appear in Section 5, and we offer a holistic view of physical mechanisms contributing to increased wintertime Mediterranean drought during recent decades including processes by which the Mediterranean region likely responds to anthropogenic greenhouse forcing.

2. Data and Methods

2.1 *Observational data and analysis period*

Global monthly SST data is based on the 5° gridded NOAA product (Smith and Reynolds 2005). We also analyze monthly 500 hPa geopotential heights for the period 1902-2008 based on the new 20th Century reanalysis data (Compo et al. 2011).

Several different gridded analyses of monthly precipitation are used. The Global Precipitation Climatology Centre analysis (GPCC; Rudolf and Schneider 2005) is

253 gridded at 1° resolution covering the period 1901-2010, and was used to construct
254 Fig. 1. The University of Delaware data (Legates and Willmott 1990) is gridded at
255 0.5° resolution and covers 1900-2008. A third data set is the Hadley Center's
256 Climate Research Unit analysis (HadCRU, Hume et al. 1998) also gridded at 0.5°
257 resolution covering 1901-2006. And finally, the Global Historical Climate Network
258 (GHCN; Vose et al. 1992) data is gridded at 5° resolution covering the period 1880-
259 2010.
260
261 Figure 2 (top) compares Mediterranean area-averaged precipitation time series for
262 the above four analyses. They broadly agree in portraying a dry period after 1970
263 which contrasts with mostly above normal precipitation during prior decades. The
264 analyses exhibit strongest agreement during 1930-1970, and the larger spread
265 among analyses during both the earlier and later decades is likely related to sparser
266 data coverage (not shown). The calculated change in area-averaged Mediterranean
267 precipitation (1971-present versus 1902-1970) as a percentage change of the
268 November to April climatology is -6.8%, -10.1%, -5.1%, and -5.1% for the GPCC,
269 UDEL, CRU, and NCDC analyses, respectively. The four data set averaged decline is
270 -6.8%.
271
272 The lower panel of Fig. 2 illustrates the density of reporting stations that have a
273 minimum of 80% available observations during the 109-yr period. There are
274 considerable monitoring gaps (e.g., the northwest Iberian Peninsula, southeast
275 Europe, and western Turkey) indicating that caution should be exercised when

assessing sub-regional structures of rainfall differences in the gridded analyses. Nonetheless, the larger-scale regional pattern of precipitation differences (1971-2010 versus 1902-1970) at the GHCN stations supports the realism of patterns constructed using the gridded analyses (cf. Fig. 1).

2.2 *Climate model simulations with realistic forcing*

Two configurations of climate model simulations are used to assess factors that may have influenced Mediterranean precipitation variability since 1902; atmospheric general circulation models (AMIP), and coupled ocean-atmosphere general circulation models (CMIP3). For the former, a total of 3 different models were available, each subjected to specified monthly varying observed global SSTs, but using climatological values for the atmospheric composition[1]. The total ensemble size of AMIP runs is 40 members. For CMIP3 simulations, a total of 22 different models were utilized, each subjected to specified monthly variations in greenhouse gases, aerosols, and half also including time varying solar irradiance and the radiative effects of volcanic activity for 1880-1999. The IPCC Special Emissions Scenario (SRES) A1B (IPCC, 2007) is used thereafter. Our analysis uses single runs

[1] The 3 atmospheric models used are the NCAR Community Climate Model (CCM3; 16-members, Kiehl et al. 1996), the NASA Seasonal-to-Interannual Prediction Project (NSIPP) model (14 members, Schubert et al. 2004a), and the Geophysical Fluid Dynamics Laboratory (GFDL) AM2.1 model (10 members, Delworth et al. 2006)

300 from each of the modeling centers yielding a total ensemble of 22 members, with the
301 model data accessed from the Program for Climate Model Diagnosis and
302 Intercomparison (PCMDI) archive as part of the Coupled Model Intercomparison
303 Project (CMIP3; Meehl et al.2007). The externally forced (greenhouse gas, aerosol,
304 solar and volcanic) signal in precipitation is estimated by averaging the multi-model
305 CMIP3 ensemble members, whereas the SST-forced signal is estimated by averaging
306 the multi-model AMIP ensemble members.
307
308 Unforced control integrations of CMIP3 coupled models are also diagnosed. Most
309 modeling centers generated roughly 300-yr simulations using climatological well-
310 mixed greenhouse gases associated with pre-1900 conditions. We calculate the
311 statistics of 109-yr precipitation change (equivalent in duration to the span of 1902-
312 2010) using 19 of the models having long integrations in order to estimate the
313 influence of internal coupled ocean-atmosphere noise.
314
315 *2.3 Climate model simulations with idealized SST forcing*
316 An additional suite of atmospheric climate model simulations are conducted that
317 specify SST anomalies representing various idealizations of the observed and CMIP3
318 simulated SST changes since 1902. The change in SSTs (1971-2010 minus 1902-
319 1970) is shown in Fig. 3 based on observations and the CMIP3 ensemble average.
320 The outstanding feature of the SST difference is an overall warming of the oceans,
321 with a generally greater tropical SST warming than that occurring over the NH
322 extratropics. Though of weaker magnitude, there is also an enhanced zonal gradient

of tropical SST warming between the Indian and Pacific Ocean. In general, the observed SST differences have stronger meridional contrast between the tropics and NH extratropics, and also a stronger zonal contrast between the Indian Ocean and the tropical Pacific Ocean. This comparison motivates a set of additional AGCM experiments using idealized SSTs forcings including (i) uniform +0.5°C warming of global SSTs, (ii) uniform +0.5°C warming of tropical (30°N-30°S) SSTs only thereby introducing a simple meridional gradient, (iii) same as (ii) but an additional 0.5°C warming of the tropical Indian Ocean thereby introducing a simple zonal gradient. We employ two models (GFDL and NASA) of the three atmospheric models used in AMIP mode, and generate respectively a 30- and 50-member ensemble subjected to the three SST forcings. The atmospheric sensitivity to the specified SST changes in these runs is determined by comparing with 50-year control integrations of each model that used a 1971-2000 climatologically averaged, seasonally varying SST.

3. Mediterranean Precipitation Variability During 1902-2010

3.1 Detection of Change

The time series of area-averaged land precipitation (30°N-45°N, 10°W-40°E) shows a different character for precipitation variability after 1970 when drought was more prevalent relative to prior decades when precipitation was consistently more abundant (Fig. 1, top). The visual impression of two different precipitation regimes during this instrumental record motivates a comparison of the spatial pattern of precipitation differences between the two epochs (1971-2010 minus 1902-1970). The results reveal widespread drying across North Africa and southern Europe extending from the Atlantic coast to the Middle East (Fig. 1, bottom).

A true change in the region's observed precipitation has *likely* occurred in a statistical sense during the last century, as revealed by comparing the observed trend with those calculated from simulations of pre-industrial unforced coupled models. We analyze continuous 109-yr integrations for each of the 19 CMIP3 models and calculate epochal differences of Mediterranean winter season precipitation in a manner analogous to what was done with the observed record. The results, plotted as a probability distribution function (PDF) in Fig. 4 (black curve), indicate that no single sample of 109-yr model time series yields a drying as strong as that observed during the 20th Century. We estimate a less than 1% probability that Mediterranean drying as strong as observed since 1902 could occur in unforced coupled models, based on analysis of the area under the curve of the non-parametric fit to the model results. This is based on using a -6.8% decline, the average of the 4 analyses. We conclude it is *unlikely* that the observed increase in drought frequency over the Mediterranean region can be attributed to internal variability alone. Our confidence language reflects the uncertainty in knowing the amplitude of the true precipitation decline and the presence of model biases in estimating the internal variability of the observed system.

3.2 Attribution of Change

We find that the recent increase in Mediterranean drought is consistent with the region's sensitivity to anthropogenic greenhouse gas and aerosol forcing, though the amplitude of the externally forced drying signal is only ½ the amplitude of observed

drying. Figure 5 shows the time series of Mediterranean cold season precipitation derived from the average of the 22 externally forced CMIP3 models (top, left), together with the spatial map of the ensemble averaged 20th Century precipitation change (bottom left). The temporally evolving signal describes increased dryness in recent decades, consistent with Mariotti et al. (2008). The precipitation decline is not gradual; the time series is noteworthy for a sudden shift to a sustained dry signal after the 1970s, a temporal behavior analogous to the observed time series (cf. Fig. 1). The spatial pattern of precipitation change in the CMIP3 ensemble consisting of a meridional dipole of North African/southern European decline and northern European increase is also similar to observations.

We find a substantial increase in the probability of a Mediterranean drying trend in the externally forced simulations relative to their likelihood of occurrence in pre-industrial unforced counterparts. A second PDF plotted in Fig. 4 (red curve) shows the Mediterranean area-averaged precipitation change (1971-2010 minus 1902-1970) simulated in each of the 22 CMIP3 models, and illustrates a reproducible drying; virtually all of the model simulations yield a reduction in precipitation during the latter decades of the 20th Century, although only one CMIP member yields a drying greater than observed. The mean values of the two PDFs are found to be statistically different at a 99.9% confidence level. When comparing the areas under the curves, we estimate a 10-fold increase in the relative probability of drying occurrences in the CMIP3 20th Century simulations versus unforced simulations that is as large as the observed drying. The detected change in Mediterranean

393 wintertime precipitation is thus attributable, in part, to the time varying external
394 radiative forcing.
395
396 Anthropogenic greenhouse gases affect Mediterranean precipitation principally via
397 a sensitivity to the contemporaneous response of the oceans to external radiative
398 forcing, rather than by an influence of local radiative forcing itself. This assessment
399 is drawn from diagnosis of the precipitation time series derived from the AMIP
400 simulations subjected only to the observed SST and sea ice variability (Fig. 5, top
401 right), and also the spatial map of the AMIP ensemble averaged 20th Century
402 precipitation change (Fig. 5, bottom right). Further supporting evidence is given in
403 Section 4 based on additional simulations using idealized features of the CMIP3 and
404 observed SST change patterns. The ocean-forced signal in the AMIP experiments is
405 one of dryness during much of the post-1970 period, analogous to the period of
406 dryness simulated in CMIP3 in response to anthropogenic greenhouse gas and
407 aerosol forcing, and also analogous to the observed post-1970 increase in drought
408 frequency. The spatial pattern of the ocean signal describes a di-pole pattern of
409 Mediterranean dry and north European wet conditions, largely reproducing the
410 pattern of the anthropogenic greenhouse gas and aerosol signal and highly
411 congruent with the observed change pattern (cf. Fig. 1).
412
413 The observed Mediterranean drying cannot be readily attributed to an observed
414 change in behavior of the North Atlantic Oscillation. First, an NAO index time series
415 for 1902-2010 fails to exhibit trend like behavior analogous to that seen for

Mediterranean rainfall, and instead exhibits only a small, and statistically insignificant, upward trend during the 109-yr period (Fig. 6, top). Second, the NAO-related signal of Mediterranean precipitation change post-1970, as estimated from a linear regression analysis, while showing drying over most of the region, has much weaker amplitudes than observed. Thus, it fails to explain the severity of overall drying, and also does not account for several regional trend features including strong drying over the eastern Mediterranean and a coincident increase in central and northern European precipitation. We note furthermore that the NAO behavior post-1970 is not materially different than that before 1970, and certainly has not changed in the dramatic manner characterizing the temporal evolution of observed Mediterranean rainfall.

It is interesting to note that our initial selection of these two epochs before and after 1970 was based purely on inspection of the observed time series of Mediterranean precipitation without any consideration of possible changes in forcings. The CMIP3 and AMIP simulations substantiate, however, that a temporal change in forcing has indeed occurred so as to distinguish pre- and post-1970, and that the key forcing involves the oceans.

A third PDF shown in Fig. 4 illustrates the statistics of precipitation trends occurring in each of the AMIP simulations (blue curve). We again find that the mean value of the PDF associated with observed ocean forcing during 1902-2010 is statistically different from that occurring in the pre-industrial unforced coupled models at 99%

confidence. However, the CMIP3 and AMIP PDFs are found not to be different at 90% confidence. We note also that, as with the CMIP results, the SST-forced drying signal is weaker than the observed drying, and only one of the AMIP members yields drying greater than was observed.

4. Mediterranean Climate Sensitivity to Idealized SST Forcing

4.1 Precipitation sensitivity

The results of section 3 indicate that SST forcing has likely been an important contributor to recent increases in Mediterranean drought. Furthermore, given the similarity between the CMIP3 and AMIP low frequency Mediterranean precipitation time series over the last century, the physics of the externally forced drying signal primarily involves forcing from the oceans.

We thus assess the sensitivity of Mediterranean wintertime precipitation to SST scenarios that reflect three gross elements of the observed global SST change during the last century (see Fig. 3); an overall global ocean warming, a greater warming of tropical oceans relative to the Northern Hemisphere (NH) extratropical oceans, and a greater warming of the tropical Indian Ocean relative to the tropical Pacific Ocean. We use a +0.5°C SST perturbation to provide a reasonable rendering of SST changes observed during the last century, although the +0.5°C enhanced warming of the Indian Ocean relative to the tropical Pacific is a factor of 4 greater than the observed gradient change since 1902, which should be kept in mind when using these additional model results to understand quantitative aspects of the AMIP and CMIP

463 simulations. We have conducted experiments with two different atmospheric
464 models (see section 2) the results of which are found to be highly consistent with
465 each other, and below we show only the results from the GFDL model.
466
467 Before discussing the results of the forced AGCM experiments, it is useful to first
468 examine the statistical relationship between these various attributes of SST change
469 and Mediterranean precipitation occurring in the separate models of the 20th
470 Century externally forced CMIP3 ensemble. We had previously shown (Fig. 3) that,
471 whereas most oceans experience a warming, neither the observed SST change nor
472 the SST response to anthropogenic greenhouse gas forcing are spatially uniform
473 patterns. Figure 7 reveals that the majority of the 20th Century CMIP3 simulations
474 generate a stronger tropical SST warming than NH extratropical SST warming, and
475 that the increase in meridional SST gradients is considerably greater than the
476 increase in zonal SST gradients. The top and bottom panels of Fig. 7 further relate
477 the simulated Mediterranean precipitation change (1971-2010 minus 1902-1970)
478 to the simulated meridional and zonal SST gradient changes, respectively. The
479 former is the difference of tropical minus NH extratropical SST change, whereas the
480 latter is the difference between tropical Indian Ocean minus tropical Pacific Ocean
481 SST change. The analysis reveals a modest linear relationship; model simulations
482 having stronger meridional and zonal increases in SST gradients tend to also
483 generate greater Mediterranean drying.
484
485 The idealized SST forcing experiments provide independent confirmation for SST

gradient-Mediterranean rainfall relationships as suggested by the empirical analyses of Fig. 7. Figure 8 (left panel) first shows the wintertime precipitation response in the SST-forced AGCM experiments for uniform +0.5°C warming of worldwide SSTs. A dry signal occurs over the eastern Mediterranean that is similar to the dry signal in that region occurring in CMIP3 and AMIP simulations. However, it is evident that such a scenario of uniform warming of +0.5°C having no changes in SST gradients cannot be invoked to explain the Mediterranean drying which spans Gibraltar to the Middle East in nature and in experiments using realistic 20th Century forcing. For a scenario of warming of +0.5°C that is restricted to tropical oceans only, a more widespread Mediterranean drying signal emerges (middle panel). A well-defined di-pole pattern having wet northern Europe and dry southern Europe also emerges in response to a tropical SST warming, one bearing strong resemblance to signals in the realistically forced model suites and also to the observed change pattern (cf. Fig. 1). Also shown in Fig. 8 (right panel) is the precipitation response to a tropical SST warming that includes a zonal contrast having stronger Indian Ocean warming than the adjacent Pacific. This additional factor yields a considerable increase in the intensity of Mediterranean drying (and also northern Europe wetness), although the spatial pattern of precipitation response is similar to the response pattern to a uniform tropical ocean warming.

4.2 Atmospheric circulation sensitivity

Regional atmospheric circulation over the North Atlantic exhibits strong sensitivity to spatial gradients in the overall SST change pattern (Fig. 9). Not surprisingly,

509 when the atmospheric model is subjected to a globally uniform SST increase the 500
510 hPa height signal is one of increased heights over the entire North
511 Atlantic/European region (top left). Yet, a modest asymmetry in the response can
512 also be discerned in which heights rise more over subtropical latitudes than over
513 the far North Atlantic. This spatial structure is made more evident by plotting the
514 residual height response which is calculated by removing the global mean height
515 anomaly from each grid point (bottom left panel). One can readily infer, from the
516 anomalous meridional gradient in the residual field, an increase in westerly flow
517 across most of the North Atlantic and Europe, and that such an onshore fetch would
518 yield increased precipitation over Europe as seen in Fig. 8.
519
520 The asymmetric character of North Atlantic height responses becomes much more
521 pronounced, and thus the associated westerly flow response becomes stronger,
522 when spatial gradients are added to the SST forcing. For instance, a distinct
523 negative 500 hPa height response emerges in simulations forced with warming
524 confined to the tropical oceans only (Fig. 9, top middle), and a well-defined
525 anomalous anticyclone now spans much of the Mediterranean region (see Fig. 9,
526 bottom middle) that is consistent with the expanded drying that envelops the entire
527 Mediterranean region in these simulations. It should be noted, however, that this
528 500 hPa height response is materially different from an NAO structure (e.g.
529 Barnston and Livezey 1987); its centers are southward shifted by nearly 10°
530 latitude compared to the NAO centers of action.
531

When an additional spatial gradient is added to the SST forcing via enhanced Indian Ocean warmth, a stronger north-south contrast in the North Atlantic height response occurs whose centers of action are more closely aligned with the NAO centers (right panels). Low pressure anomalies occur over the Arctic while opposite signed anomalies occur over the central North Atlantic as typically is seen with positive index phases of the NAO, although the zonal scale of the height response is much greater than what occurs during NAO events. We also find a pronounced northward shift and an intensification of storm track anomalies in these experiments (2.5-6 day band pass 500 hPa height variances, not shown) that mimic the North Atlantic storm track anomalies associated with the positive NAO phase (e.g. Hurrell 1995). These dynamically driven synoptic-eddy effects are likely instrumental in explaining the substantial increase in western Mediterranean drying occurring in the warmed Indian Ocean scenario experiment compared to either the globally uniform or tropically uniform warming experiments (see Fig. 8, right).

Several aspects of the Mediterranean climate sensitivity revealed in these idealized SST forcing experiments are germane to understanding the recent observed drying in that area. A globally uniform +0.5°C warming alone produces drying of the eastern Mediterranean, and this may identify a major factor responsible for the strong observed eastern Mediterranean drying. Furthermore, a zonally uniform warming of +0.5°C of tropical SSTs alone renders widespread Mediterranean drying, and these model results may point to a major factor for the observed Mediterranean-wide drying which has taken place in concert with an observed

555 +0.5°C greater tropical SST warming relative to the extratropical oceans since 1902.
556 Neither of these SST forcings excite an atmospheric response resembling the NAO
557 pattern, and thus fails to describe one aspect of the observed (based on re-analysis
558 data) circulation change since 1902. The atmospheric responses in these
559 simulations do, however, generate regional circulation patterns suggestive of storm
560 track shifts conducive for Mediterranean dryness. An *isolated, and regionally*
561 *enhanced* Indian Ocean warming is thus not a sole, nor even a necessary pattern for
562 oceanic forcing of Mediterranean drying. The final simulation suite indicates that an
563 SST condition that includes a stronger Indian Ocean warming relative to adjacent
564 oceans is conducive for generating a North Atlantic/European regional circulation
565 pattern resembling the positive polarity of the NAO, which enhances the regional
566 drying especially of the western Mediterranean (see Fig. 7). The modest upward
567 trend of an index of the NAO since 1902 may thus be consistent with the influence of
568 such remote forcing. Similarly, the lack of such an NAO trend in the CMIP
569 simulations also appears to be physically consistent with the more uniform increase
570 of SSTs throughout the tropics that occurs in response to external radiative forcing
571 since 1902 in those models. Section 5 further discusses the connections among
572 Mediterranean drying, Indian Ocean SST forcing, NAO variability, and links to
573 anthropogenic forcing.
574
575 The above interpretation of the Mediterranean drying invokes the notion of
576 teleconnections having strong regional expression, but theories of anthropogenic
577 climate change also include the expectation for a poleward expansion of the

578 subtropical dry zones through mechanisms involving the zonal mean circulation.
579 To what extent is the Mediterranean drying occurring in these idealized SST forcing
580 experiments simply a response to a poleward expansion of the model's Hadley cell?
581 The model simulations for the globally uniform warming indeed exhibit a significant
582 poleward shift of the northern edge of the Hadley cell during November-April which
583 contributes to the drying of lower mid-latitudes (not shown). However, there is
584 little further Hadley cell change in the runs that involve the addition of SST
585 gradients (not shown), and thus the envelopment of all the Mediterranean in
586 dryness and with greater intensity in these simulations is primarily due to
587 mechanisms of regional teleconnection processes rather than zonally symmetric
588 dynamics.
589
590 *4.3 Comparison with CMIP3, AMIP, and observations*
591 Principal features of CMIP3, AMIP, and observed 20th Century tropospheric height
592 changes can be understood in the framework of our simplified forcing experiments.
593 Figure 10 shows the height change simulated in CMIP3 (left) and AMIP (center), and
594 observed (right), while Table 1 presents the 500 hPa height pattern correlations
595 (computed over the map domains of Figs. 9 and 10) of each SST scenario with the
596 CMIP3, AMIP, and observed change patterns. For CMIP3, the relatively uniform
597 increase in North Atlantic/European 500 hPa heights is consistent with the
598 relatively uniform pattern of SST change simulated in response to anthropogenic
599 greenhouse gas forcing. The modest amplitude asymmetric component of the
600 CMIP3 residual height change pattern consists of local minima over the North

601 Atlantic and eastern Europe that are very similar to those occurring in the globally
602 uniform and also the tropically uniform warming runs; they are materially different,
603 however, from those occurring in the idealized SST runs subjected to enhanced
604 Indian Ocean warming. Table 1 indicates a 0.60 and 0.83 pattern correlation of
605 CMIP3 with height responses in the globally uniform and tropically uniform SST
606 warming runs, respectively, but only a 0.18 correlation with the height response in
607 the enhanced Indian Ocean warming experiments.
608
609 In contrast, the AMIP simulations (Fig. 10, middle panels) yield a 20th Century
610 circulation change that projects more strongly on an NAO structure, and in this
611 sense is most similar to the height response occurring in the idealized SST runs
612 using enhanced Indian Ocean warming. We note also that the zonal scale of the
613 height change pattern in AMIP is considerably larger than what occurs during NAO
614 events, yet appears consistent with a footprint attributable to an influence of Indian
615 Ocean SST warming. Table 1 indicates a 0.86 pattern correlation between the AMIP
616 height change pattern and the height response in the enhanced Indian Ocean
617 warming runs, whereas little spatial agreement exists with the height responses in
618 the other two idealized SST experiments. A similar assessment pertains to the
619 observed height change pattern. The 20th Century reanalysis data indicates a height
620 change pattern since 1902 that also projects onto a positive NAO pattern. Table 1
621 confirms that this most resembles the forced response involving enhanced warming
622 of the Indian Ocean with a 0.61 pattern correlation, whereas appreciably weaker
623 correlations of about 0.3 describe the agreement with height anomaly patterns in

624 the other two experiments.

625

626 **5. Conclusions**

627 *5.1. Summary*

628 Our results indicate that a change in the Mediterranean region's cold season
629 precipitation has *likely* occurred over the period 1902-2010. The direction of this
630 change has been toward drier conditions, with increased drought frequency after
631 about 1970. Our confidence language reflects uncertainties in the magnitude of the
632 actual observed drying, and possible biases in unforced coupled model estimates of
633 natural internal variability. The results further indicate that the detected change
634 toward drier conditions is attributable, *in part*, to the Mediterranean region's
635 sensitivity to time evolving external radiative forcing. The *amplitude* of the
636 externally forced, area averaged Mediterranean drying signal (estimated from the
637 ensemble mean of CMIP3 simulations) is roughly ½ the magnitude of the observed
638 drying, indicating that other processes likely also contributed to the observed
639 drying. Regarding mechanisms for Mediterranean drying, our analysis of AMIP
640 simulations reveals that SST forcing alone yields a signal of Mediterranean drying
641 whose spatial signature and temporal evolution capture several elements of both
642 observations and the CMIP3 externally forced signal. SST forcing has thus *likely*
643 played an important part in the observed Mediterranean drying, and the externally
644 forced drying signal *likely* also occurs through the impact of an SST change signal.

645

646

647

This line of reasoning motivated further experimentation in which atmospheric models were subjected to idealized forcings describing several gross features of global SST change during the last century. A uniform +0.5°C warming of the global oceans induced strong drying over the eastern Mediterranean region, but was ineffective in producing the distinctive pattern of a widespread Mediterranean drying trend occurring in observations, CMIP3 and AMIP simulations for 1902-2010. Instead, meridional and zonal gradients in the SST change pattern were shown to be necessary to induce a Mediterranean precipitation response having a single sign that spanned Gibraltar to the Middle East. For +0.5°C warming confined to tropical latitudes only (thereby introducing an enhancement of the climatological meridional gradient), drying envelops the entire Mediterranean region. A regional atmospheric circulation response in these uniform warming runs, resembling the CMIP3 simulated circulation change pattern, is of a type that, though different from an NAO pattern, is conducive for displacing moisture bearing storms northward into the European continent. The intensity of this drying increases substantially, especially over the western Mediterranean, when the tropical Indian Ocean is warmed +0.5°C more than the rest of the tropical oceans (thereby introducing an enhancement of the climatological zonal gradient). For this latter forcing scenario, the atmospheric response pattern was shown to project onto the positive phase of the NAO. Although this additional Indian Ocean warmth exaggerates the magnitude of observed warming of the Indian Ocean relative to the Pacific Ocean during the past century, the experimental results may nonetheless point to a factor

671 contributing to the modest upward trend in an NAO index in observations and AMIP
672 simulations during 1902-2010, and may also account for the lack thereof in the
673 CMIP3 ensemble mean (which produced very little zonal gradient in the tropical SST
674 response to external radiative forcing). Of course, other processes can also induce
675 low frequency variability of North Atlantic atmospheric circulation, and the
676 possibility that the modest amplitude observed upward trend toward a positive
677 phase of the NAO was due to internal atmospheric variability alone cannot be
678 discounted.
679
680 *5.2 Discussion*
681 In reconstructing a history of Mediterranean climate since 1902 and in determining
682 the causes for its change we have relied upon various sources. The description of
683 precipitation change itself is not without its difficulties given the rather sparse
684 network of long-term observations, and while 4 different analyses agree that a large
685 spatial average of Mediterranean land precipitation has almost certainly declined
686 during 1902-2010, the intensity of that decline is less certain. The description of the
687 atmospheric circulation change at 500 hPa was based upon a reanalysis data set that
688 assimilated only surface pressure reports and used monthly SST and sea ice
689 distributions (Compo et al. 2011). The authors' assessment of that data indicate a
690 particularly high quality of extratropical NH circulation features that is comparable
691 to that of current three-day operational numerical weather prediction forecasts. The
692 use of lower boundary forcings to constrain the assimilating model implies that the
693 long-term change estimated from the reanalysis is not strictly independent of AMIP
694 or CMIP-style simulations of change, though it is very likely that the use of observed

695 sea level pressure data provides the major constraint for extratropical circulation in
696 the reanalysis data. We thus have high confidence that the reanalysis and climate
697 simulations are independent sources of information regarding the region's climate
698 change since 1902, and that these simulations provide a meaningful appraisal of
699 probable causes for the increase in Mediterranean drought frequency.
700
701 Our results indicate that similar physical processes have likely contributed to
702 observed and CMIP3 simulated Mediterranean wintertime drying (i.e., SST forcing
703 and atmospheric teleconnections), although some details of the SST change since
704 1902 differ between observations and the CMIP3 externally forced signal that
705 impact details of the regional atmospheric response patterns. Regarding this latter
706 issue, our results suggest that the Indian Ocean may have played a greater role in
707 the observed Mediterranean drying than occurs in CMIP3, including the rendering of
708 an NAO circulation response in observations that is lacking in CMIP3. The
709 importance of positive SST anomalies over the Indian Ocean warm pool for
710 widespread Mediterranean drought associated with a regional NAO response has
711 been shown in several prior studies (e.g. Hoerling et al. 2001; Bader and Latif 2003;
712 Lu et al. 2004; Hoerling et al. 2004; Li et al. 2006), and our results are consistent
713 with those. A new feature of the simulations conducted here is that Indian Ocean
714 warming, when immersed in a pattern of uniform warming of the world oceans or of
715 uniform warming of the tropical oceans, is ineffective in generating an NAO-like
716 response pattern. Thus, to the extent the true anthropogenic signal of SST change
717 during 1902-2010 is one of uniform warming, an NAO-like atmospheric change is

718 not an expectation (at least based on SST forcing considerations alone), and this
719 helps to explain the lack of an NAO signal in CMIP3. Yet, the observed SST change
720 since 1902, contrary to the signal of SST change estimated from the ensemble of
721 CMIP3 runs, does possess an appreciably stronger Indian Ocean warming than
722 occurring over the tropical Pacific, a condition that our idealized SST experiments
723 and those in prior studies indicates would favor an NAO-like response. In this
724 regard, the AMIP simulations driven by observed SST variations simulate the
725 observed 500 hPa height change pattern better than do the CMIP3 simulations
726 driven by external radiative forcing. We thus conclude that observed NAO-like
727 circulation change is reconcilable with a fingerprint of regional sensitivity to
728 enhanced Indian Ocean warming (relative to the tropical Pacific), consistent with
729 previous studies.
730
731 Despite this ability to explain the behavior in the fully forced time varying climate
732 simulations, some uncertainty must necessarily remain regarding a full
733 understanding of how, and by how much, anthropogenic forcing contributed to
734 *observed* Mediterranean drying during 1902-2010. It is especially unclear to what
735 extent the observed zonal contrast in tropical SST warming, which contributes to
736 drying via an NAO teleconnection link, is due to internal variability or is an
737 expression of nature's response of anthropogenic forcing. There is no evidence that
738 indicates the anthropogenic signal of the tropical ocean response is one of stronger
739 Indian Ocean warming relative to the Pacific Ocean. It is plausible that
740 observational indications for an enhance zonal gradient is linked to a weaker

741 warming in the tropical Pacific resulting from a particularly strong occurrence of
742 internal variability in that region (rather than an enhanced anthropogenic warming
743 signal over the Indian Ocean), as suggested by results of Knutson et al. (2006) and
744 more recently by Hoerling et al. (2010). On the other hand, it is also plausible that
745 CMIP3 models have biases in their SST response to GHG forcing, especially over the
746 tropical Pacific (e.g. Vecchi et al. 2008) and that the true tropical ocean response
747 deviates appreciably from the ensemble mean of CMIP3 simulations. This line of
748 reasoning would argue that an anthropogenic drying signal of the Mediterranean
749 region is stronger than inferred from the CMIP3 ensemble mean simulations.
750
751 A key point that our results raise, however, is that the link between anthropogenic
752 forcing and observed Mediterranean drying during the analysis period of 1902-
753 2010 does not require a connection involving *enhanced* Indian Ocean warming nor a
754 North Atlantic Oscillation circulation response---a uniform warming of the tropical
755 oceans alone induces widespread drying. The stronger observed drying occurring
756 since 1902 (than in the CMIP3 ensemble) may result from an internally generated
757 component of SST variability over the tropical Pacific, where a minimum of warming
758 has acted to intensify the tropical-wide SST contrast in such a manner that favors
759 forcing of a trend toward the positive NAO phase. The stronger observed drying
760 may also merely reflect the serendipitous contribution by internal atmospheric
761 variability. Each of these internal factors, or a combination of them, could have
762 enhanced the Mediterranean's drying in observations above and beyond the
763 anthropogenic signal derived from the CMIP3 ensemble mean.

764

765 Uncertainties in the SST analyses themselves, however, do not permit a more
766 definitive assessment of the difference between observed and CMIP3 SST gradients
767 across the Indo-Pacific region. Various historical analyses lead to differences in the
768 magnitudes of zonal gradients in SST (Deser et al. 2010). It is nonetheless
769 reasonable to believe that an appreciable west-east gradient in tropical SST change
770 exists in light of the agreement between AMIP and observed circulation changes, in
771 the form of a positive NAO structure. This agreement may be a proxy indicator for a
772 greater Indian Ocean warming compared to the tropical Pacific warming as implied
773 also by the results of our idealized SST sensitivity experiments.

774

775 There are further questions concerning Mediterranean drought to which our
776 analysis applies, though which cannot be answered based on the current results
777 alone. In particular, what is the actual intensity of the anthropogenic drying signal
778 over the Mediterranean region? The observed drying has been roughly double the
779 ensemble mean CMIP3 drying, and only one of the 22 models generate a drying as
780 strong as observed. We have already addressed the fact that the true amplitude of
781 the observed drying is not known, and thus the difference with CMIP3 amplitudes
782 cannot be absolutely determined. It is nonetheless plausible that the observed
783 change may include a substantial internal variability component that is
784 coincidentally of the same polarity as the climate change signal. Indeed, the spread
785 of PDFs in Fig. 4 attests to the considerable amplitude of internally generated
786 centennial scale variations of Mediterranean precipitation trends. It is also possible

787 that the true climate change signal is stronger than implied by the CMIP3 ensemble
788 mean. For instance, if the climate change signal of tropical SST change involves a
789 stronger zonal SST gradient across the Indo-Pacific than simulated in CMIP3, but
790 akin to observations, an intensified Mediterranean drying signal would be expected.
791 This line of reasoning would argue that the amplitude of the CMIP3 drying signal is
792 erroneously weak owing to biases in the coupled model's global SST response. Yet,
793 our AMIP results also generate a drying signal that is only about ½ the amplitude of
794 the observed drying, and they also contain only one simulation (of 40) that has a
795 drying trend greater than observed. Further climate simulations studies are
796 required to clarify these matters. It is expected that climate models to be used in
797 support of the next IPCC Assessment, for instance, will use considerably higher
798 spatial resolution than those used in CMIP3 and in our study. It will be useful to
799 repeat the current analysis with them, and especially to conduct parallel large
800 ensemble suites of CMIP and AMIP style integrations that use the same atmospheric
801 models.
802
803 A second question concerns the sub-regional precipitation signals of climate change.
804 We have already indicated that the observational data are not adequate to assess
805 centennial changes at local scales. There are nonetheless tantalizing indications of
806 particularly strong drying over portions of southern Spain, Morocco, northern
807 Algeria, and portions of the Middle East where select stations are available (see Fig.
808 2). These are among the areas we have found to be especially drought sensitive
809 when Indian Ocean warming is enhanced, raising the scientific need to further

understand how climate change will affect the detailed pattern of SST change. The question is of considerable practical importance also in light of assessments for current and projected 2025 water scarcity in the Mediterranean (Mediterranean Water Scarcity and Drought Working Group 2007). It is estimated that water withdrawals ---unrelated to climate change--- will alone exceed the average annual volume of renewable natural water resources in Spain's Mediterranean basin, North Africa, and the eastern Mediterranean by 2025. A climate change induced drying will clearly aggravate a significant water resource challenge for the area, and information on the sub-regional patterns of climate change will be important in assisting a planning framework for societal responses to drought.

Acknowledgements. The authors thank the Editor and three anonymous reviewers for their constructive comments that improved the content of this paper. We gratefully acknowledge the LaMont-Doherty Earth Observatory of Columbia University for access to the CCM3 AMIP ensemble, NOAA's GFDL for access to the AM2.1 AMIP ensemble, and NASA's GMAO Goddard Space Flight Center for access to the NASA AMIP ensemble. We also acknowledge the modeling groups, the Program for Climate Model Diagnosis and Intercomparison (PCMDI) and the WCRP's Working Group on Coupled Modelling (WGCM) for their roles in making available the WCRP CMIP3 multi-model dataset. Support of this dataset is provided by the Office of Science, U.S. Department of Energy. This study is supported in part by funds from the NOAA Office of Global Programs Climate Variability Program.

6. References

Bader, J, and M. Latif, 2003: The impact of decadal-scale Indian Ocean SST anomalies on Sahelian rainfall and the North Atlantic Oscillation. *Geophys. Res. Lett.,* **30**, DOI 10.1029/2003GL018426.

Barnston, A., and R. Livezey, 1987: Classification, seasonality, and persistence of low frequency atmospheric circulation patterns. *Mon. Wea. Rev*., **115**, 1083-1126.

Compo, G.P., J.S. Whitaker, P.D. Sardeshmukh, N. Matsui, R.J. Allan, X. Yin, B.E. Gleason, R.S. Vose, G. Rutledge, P. Bessemoulin, S. Brönnimann, M. Brunet, R.I. Crouthamel, A.N. Grant, P.Y. Groisman, P.D. Jones, M. Kruk, A.C. Kruger, G.J. Marshall, M. Maugeri, H.Y. Mok, Ø. Nordli, T.F. Ross, R.M. Trigo, X.L. Wang, S.D. Woodruff, and S.J. Worley, 2011: The Twentieth Century Reanalysis Project. *Quarterly J. Roy. Meteorol. Soc*., **137**, 1-28. DOI: 10.1002/qj.776.

Davis, S. M., and K. H. Rosenlof, 2011: A multi-diagnostic intercompariosn of tropical width time series using reanalyses and satellite observations, *J. Climate*, doi: 10.1175/JCLI-D-11-00127.1

Delworth, T. L., et al., 2006: GFDL's CM2 global coupled climate models. Part I: Formulation and simulation characteristics, *J. Climate*, **19**, 643-674, doi:10.1175/JCLI3629.1.

Deser, C., A. Phillips, and M. Alexander, 2010: Twentieth century tropical sea surface temperature trends revisted. *Geophys. Res. Lett.,* **37**, L10701, doi:10.1029/2010GL043321.

ESPERE, 2006: Climate Encyclopedia-Food and Climate. Available at http://espere.mpch-mainz.mpg.de/documents/pdf/

858 Gillett, N.P., 2003. Climate change and the North Atlantic Oscillation. In: Hurrell, J.W.,
859 Kushnir, Y., Ottersen, G., Visbeck, M. (Eds.), The North Atlantic Oscillation,
860 Climatic Significance and Environmental Impact. AGU Geophys.Monogr., vol.134,
861 pp.193–209.
862 Giorgi, F., Climate change hot spots. *Geophys. Res. Lett.*, **33**, L08707,
863 doi:10.1029/2006GL025734.
864 Hoerling, M. P., J. Hurrell, and T. Xu, 2001: Tropical origins for North Atlantic
865 climate change. *Science*, **292**, 90-92.
866 Hoerling, M. P., and A. Kumar, 2003: The perfect ocean for drought. *Scienc*e, **299**,
867 691-694.
868 Hoerling M.P., J. W. Hurrell , T. Xu , G. T. Bates, and A. Phillips, 2004: Twentieth
869 Century North Atlantic climate change. Part II: Understanding the effect of Indian
870 Ocean warming. *Climate Dyn.*, **23**, 391-405.
871 Hulme,M., Osborn,T.J. and T.C.Johns (1998) Precipitation
872 sensitivity to global warming: Comparison of observations with
873 HadCM2 simulations. *Geophys. Res. Letts.,* **25**, 3379-3382.
874 Hurrell, J. W., 1995: Decadal trends in the North Atlantic Oscillation: Regional
875 temperatures and precipitation. *Science*, **269**, 676-679.
876 Hurrell J.W., M. P. Hoerling, A. Phillips, and T. Xu, 2004: Twentieth Century North
877 Atlantic climate change. Part I: Assessing determinism. *Climate Dyn*. **23**, 375-390.
878 Hurrell, J. W., and C. Deser, 2009: North Atlantic climate variability: The role of the
879 North Atlantic Oscillation. *J. Mar. Syst.*, **78**, No. 1, 28,
880 DOI:10.1016/j.jmarsys.2008.11.026.

881 IPCC, 2007: Summary for Policymakers. In: *Climate Change 2007: The Physical*
882 *Science Basis. Contribution of Working Group I to the Fourth Assessment Report of*
883 *the Intergovernmental Panel on Climate Change* [Solomon, S., D. Qin, M. Manning,
884 Z. Chen, M. Marquis, K.B. Averyt, M.Tignor and H.L. Miller (eds.)]. Cambridge
885 University Press, Cambridge, United Kingdom and New York, NY, USA.
886 International Food Policy Research Institute (IFPRI), 2009: "Climate Change:
887 Impact on Agriculture and Costs of Adaptation", Food Policy Report, Washington
888 DC, September 2009.
889 Jones, P., T. Osborn, and K. Briffa, 2003: Pressure-based measures of the North
890 Atlantic Oscillation (NAO): A comparison and an assessment of changes in the
891 strength of the NAO and its influence on surface climate parameters. In: Hurrell,
892 J.W.,Kushnir, Y., Ottersen, G., Visbeck, M. (Eds.), The North Atlantic Oscillation,
893 Climatic Significance and Environmental Impact. AGU Geophys.Monogr., vol.134,
894 pp.51–62.
895 Kiehl, J., J. Hack, , G. Bonan, B. Boville, D. Williamson, and P. Rasch, 1998: . The
896 National Center for Atmospheric Research Community Climate Model: CCM3. *J.*
897 *Climate*, **11**, 1131-1149.
898 Knutson, T., and Coauthors, 2006: Assessment of twentieth century regional surface
899 temperature trends using the GFDL CM2 coupled models. *J. Climate*, **19**, 1624-
900 1651.
901 Legates, D. R. and C. J. Willmott, 1990: Mean Seasonal and Spatial Variability Global
902 Surface Air Temperature. *Theoretical and Applied Climatology* , **41**, 11-21.
903 Li, S, M Hoerling, and S. Peng: 2006: Coupled ocean-atmosphere response to Indian

904 Ocean warmth. *Geophys. Res. Letters*, **33**, L07713, doi:10.1029/2005GL025558.
905 Lu J, Greatbatch RJ, Peterson KA , 2004: Trend in Northern Hemisphere winter
906 atmospheric circulation during the last half of the twentieth century. *J. Climate*
907 **17**, 3745–3760.
908 Lu, J., G. Vecchi, and T. Reichler, 2007: Expansion of the Hadley cell under global
909 warming. *Geophys. Res. Lett.,* **34**, L06805, doi:10.1029/2006GL028443.
910 Mariotti, A., N. Zeng, J.-H. Yoon, V. Artale, A. Navarra, P. Alpert, and L. Z. X. Li, 2008:
911 Mediterranean water cycle changes: Transition to drier 21st century conditions
912 in observations and CMIP3 simulations. *Environ. Res. Lett.*, **3**, 044001, doi:10.
913 1088/1748-9326/3/4/044001.
914 Mariotti, A., 2010: Recent Changes in the Mediterranean Water Cycle: A Pathway
915 toward Long-Term Regional Hydroclimatic Change? *J. Climate*, **23**, 1513-1525, doi:
916 10.1175/2009JCLI3251.1
917 Matiotti, A., and A. Dell'Aquilla, 2011: Decadal climate variability in the
918 Mediterranean region: roles of large-scale forcings and regional processes. *Clim.*
919 *Dyn.*, doi: 10.1007/s00382-011-1056-7.
920 Mediterranean Water Scarcity and Drought Working Group, 2007: Technical report
921 on water scarcity and drought management in the Mediterranean and the water
922 framework directive. Mediterranean EU Water Initiative/Water Framework
923 Directive Joint Process, Brussels, April 2007.
924 Meehl, G. , and Coauthors, 2007: The WCRP CMIP3 multimodel dataset: A new era in
925 climate change research. *Bull. Amer. Met. Soc.*, **88**, 1384-1394.

926 Mehta V., M. Suarez , J. Manganello , and T. Delworth , 2000: Oceanic influence on
927 the North Atlantic Oscillation and associated Northern Hemisphere climate
928 variations: 1959–1993. *Geophys. Res. Lett.*, **27**, 121–124
929 Osborn, T., 2011: Variability and changes in the North Atlantic Oscilltion index. In:
930 Hydrological, Socioeconomic and Ecological Impacts of the North Atlantic
931 Oscillation in the Mediterranean Region, book in press.
932 Previdi, M., and B. G. Liepert, 2007: Annular modes and Hadley cell expansion under
933 global warming. *Geophys. Res. Lett.,* **34**, L22701, doi:10.1029/2007GL031243.
934 Robertson A., C. Mechoso, Y. Kim, 2000: The influence of Atlantic sea surface
935 temperature anomalies on the North Atlantic Oscillation*. J. Climate*, **13**, 122–
936 138.
937 Rudolf, B., and U. Schneider, 2005: Calculation of gridded precipitation data for the
938 global land-surface using in-situ guage observations. In: *Proceedings of the 2nd*
939 *Workshop of the International Precipitation Working Group (IPWG),* Monterey,
940 October 2004, pp. 231-247.
941 Seager, R., N. Naik and G. A. Vecchi, 2010: Thermodynamic and dynamic
942 mechanisms for large-scale changes in the hydrological cycle in response to
943 global warming. *J. Climate*, **23**, 4651-4668.
944 Seager, R., and Coauthors, 2007: Model projections of an imminent transition to a
945 more arid climate in southwestern North America. *Science*, **316**, 1181-1184.
946 Solomon, S., D. Qin, M. Manning, Z. Chen, M. Marquis, K. B. Averyt, M. Tignor, and H.
947 L. Miller, 2007: Climate Change 2007: The Physical Science Basis. Cambridge
948 University Press, 996 pp.

949 Schubert, S.D., M. J. Suarez, P. J. Pegion, R. D. Koster, and J. T. Bacmeister , 2004: On
950 the Cause of the 1930s Dust Bowl, *Science,* **33**, 1855-1859.
951 Smith, T. M., and R. W. Reynolds , 2005: A global merged land air and sea surface
952 temperature reconstruction based on historical observations (1880-1997), *J.*
953 *Climate*., **18**, 2021-2036.
954 Sutton R., W. Norton, and S. Jewson, 2001: The North Atlantic Oscillation - What role
955 for the Ocean? *Atm Sci Lett*, DOI 10.1006/asle.2000.0018
956 Ulbrich, U., and Coauthors, 2006: The Mediterranean climate change under global
957 warming. Mediterranean Climate Variability and Predictability, P. Lionello et al.,
958 Eds., Elsevier, 398–415.
959 Vecchi, G. A., A. Clement, and B. J. Soden, 2008: Pacific signature of global warming:
960 El Niño or La Niña?, *Eos* Trans. AGU, 89(9),doi:10.1029/2008EO090002.
961
962 Vose, R. S., R. L. Schmoyer, P. M. Steurer, T. C. Peterson, R. Heim, T. R. Karl, and J. K.
963 Eischeid, 1992: The Global Historical Climatology Network: Long-term monthly
964 temperature, precipitation, sea-level pressure, and station pressure data. Rep.
965 ORNL/CDIAC-53, Carbon Dioxide Inf. Anal. Cent., Oak Ridge Natl. Lab., Oak Ridge,
966 TN, 25pp.[Available from Carbon Dioxide Information Analysis Center,
967 Oak Ridge National Laboratory, Oak Ridge, TN, 37831-6335].
968 Wunsch, C., 1999: The interpretation of short climate records, with comments on
969 the North Atlantic Oscillation and Southern Oscillations. *Bull. Amer. Meteor. Soc*.,
970 **80**, 245-255.
971 Yin, J. H., 2005: A consistent poleward shift of the storm tracks in simulations of 21st

century climate. *Geophys. Res. Lett.*, **32,** L18701, doi:10.1029/2005GL023684.

Zhang, X., F. W. Zwiers, G. C. Hegerl, F. H. Lambert, N. P. Gillett, S. Solomon, P. A. Stott and T. Nozawa , 2007: Detection of human influence on twentieth-century precipitation trends. *Nature*, **448**, 461-465.

Figure captions:

Figure 1. Observed time series of Mediterranean (30N-45N; 10W-40E) cold season (Nov-Apr) precipitation for the period 1902-2010 (top) and the observed change in cold season precipitation for the period 1971-2010 minus 1902-1970 (bottom). Anomalies (mm) are relative to the 1902-2010 period. Solid curve is the smoothed precipitation time series using a 9-pt Gaussian filter. Data is from the Global Precipitation Climatology Center (GPCC).

Figure 2. Time series of Mediterranean (30N-45N; 10W-40E) cold season (Nov-Apr) precipitation for the period 1902-2010 (top) for four observed data sets: GPCC (Global Precipitation Climatology Center), GHCN (Global Historical Climatology Network), UDEL (University of Delaware), CRU (Climatic Research Unit). Anomalies (mm) are referenced to the 1902-2010 period and are smoothed with a 9-pt Gaussian filter. The bottom panel shows a station-based analysis of the change in cold season precipitation for the period 1971-2010 minus 1902-1970; stations are extracted from the GHCN (monthly) and GHCN-d (daily) datasets.

Figure 3. Cold season (Nov-Apr) sea surface temperature departures (°C) for the period 1971-2010 minus 1902-1970. Top panel: observed analysis from the NOAA merged gridded data set. Bottom panel: Multi-model CMIP3 ensemble sea surface temperatures based on 22 IPCC models.

Figure 4. Probability distribution functions (PDFs) for the 1971-2010 minus 1902-1970 period anomalies of cold season precipitation over the Mediterranean region as % of climatology. The red curve is based on the analysis of 22 IPCC models, while the blue curve is based on 40 AMIP simulations of the 20th century. The solid black curve is drawn from the analysis of 109-yr long samples of unforced integrations from 19 IPCC simulations using pre-industrial concentrations of greenhouse gases. The observed precipitation index decline, based on the average of four analyses (-6.8%) is shown by the gray tick mark to the left. Colored tick marks indicate individual ensemble members.

Figure 5. Simulated change in cold season precipitation (mm) over the Mediterranean region as in Figure 1 based on the ensemble average of 22 IPCC models (left) and the ensemble average of 40 AMIP 20th century runs (right). The difference plots in the lower panels are for the period 1971-2010 minus 1902-1970.

Figure 6. Time series of an index of the observed North Atlantic Oscillation (NAO) during the cold season (Nov-Apr) for the period 1902-2010 (top) and the change in cold season precipitation for the period 1971-2010 minus 1902-1970 that is linearly related to the change in the NAO index (bottom). NAO index is the principal component time series of the leading empirical orthogonal function of monthly 500 hPa heights during Nov-April over the region 20°N-90°N, 120°W-60°E. Data is the 20th Century Reanalysis, and solid curve is the smoothed NAO time series using a 9-pt Gaussian filter. The precipitation impact (mm) of the NAO change is derived by

regressing Nov-Apr precipitation onto the NAO index, and then scaling by the mean difference of the NAO index between the two periods (+0.2 standardized units).

Figure 7. Relationship between the change (1971-2010 minus 1902-1970) in cold season Mediterranean precipitation (mm) and sea surface temperatures gradient (°C) for the 22 IPCC models. Top panel: Area averaged precipitation versus the meridional (30N-60N minus 30S-30N) SST gradient. Bottom panel: As above but for the zonal (tropical Indian ocean minus tropical Pacific) zonal SST gradient. In both panels the observed value is indicated by the solid red dot.

Figure 8. Forced response of cold season (Nov-April) precipitation (mm) to three SST scenarios. The forced response is the average of 30 simulations using each of three scenarios of changes in SST's: left, uniform warming of +0.5C; middle, warming of +0.5C in the tropics only; right, warming of +1C over the Indian Ocean with +0.5C warming elsewhere in the tropics.

Figure 9. As in Figure 8 but for the forced response of 500 hPa heights (gpm) to the three SST scenarios. The top panel shows the total height anomaly while the bottom panel shows the residual (global mean removed) height anomaly.

Figure 10. Cold season (Nov-April) 500 hPa height departures (gpm) for the period 1971-2010 minus 1902-1970 for the 22 model IPCC ensemble average (left), the 40 run ensemble average of 20th century AMIP runs (middle), and based on 20th

Century Reanalysis (right). Total height changes are shown in the top panels and the residual fields (with global mean height anomaly removed) below.

Table 1. *The spatial correlation of 500 hPa height anomaly patterns for the North Atlantic/European region of the map domains shown in Figs. 8 and 9. The height responses in the atmospheric model simulations using idealized SST forcings (top row) are compared to the 20th Century height change patterns in the realistically forced model experiments and observations (left column)*

	Pattern Correlations for 500 hPa Height Responses		
	Uniform Global SST Warming	*Uniform Tropical SST Warming*	*Enhanced Indian Ocean Warming*
CMIP3	0.60	0.83	0.18
AMIP	0.17	0.21	0.86
OBS	0.32	0.29	0.61

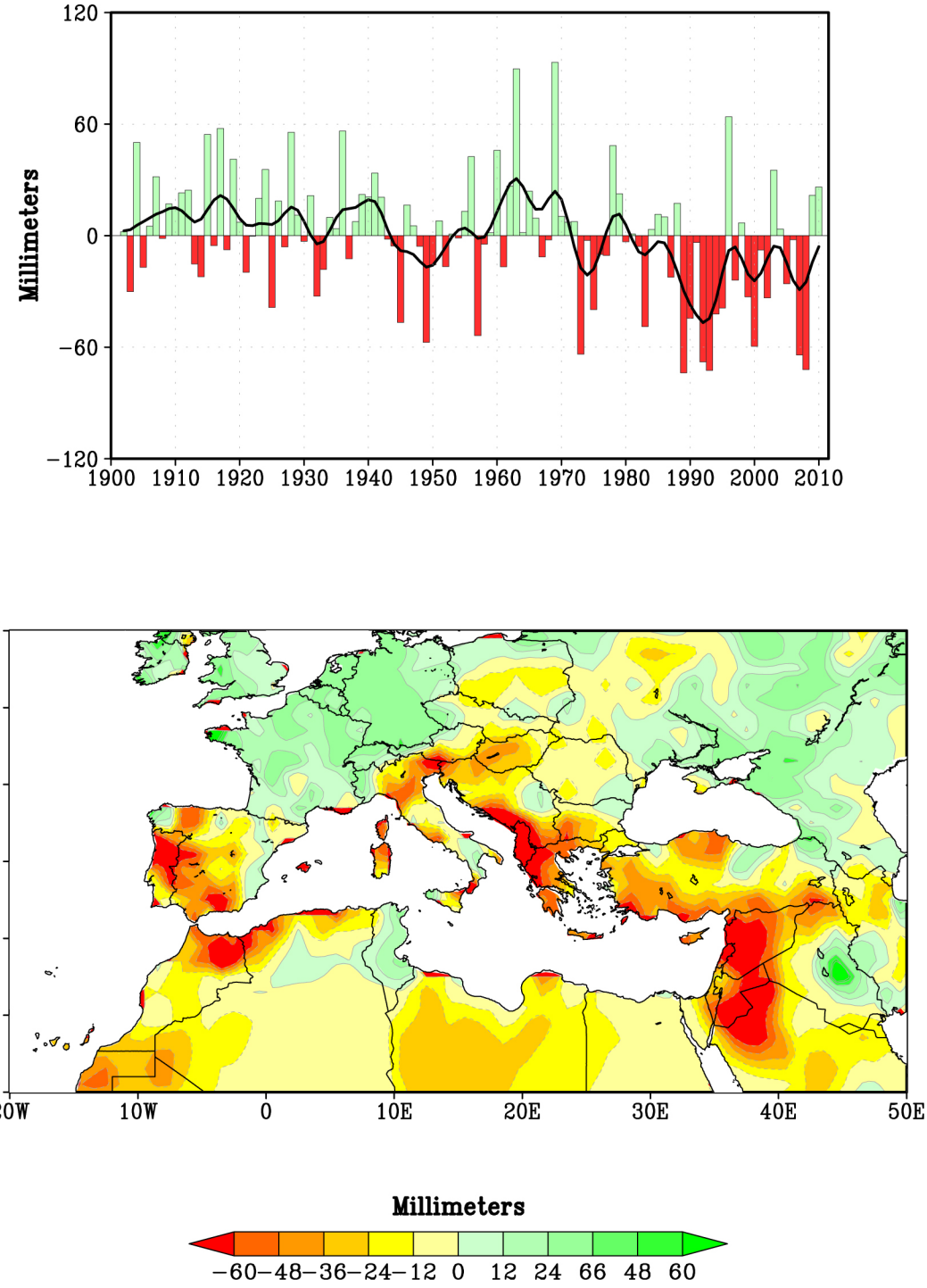

Figure 1. *Observed time series of Mediterranean (30N-45N; 10W-40E) cold season (Nov-Apr) precipitation for the period 1902-2010 (top) and the observed change in cold season precipitation for the period 1971-2010 minus 1902-1970 (bottom). Anomalies (mm) are relative to the 1902-2010 period. Solid curve is the smoothed precipitation time series using a 9-pt Gaussian filter. Data is from the Global Precipitation Climatology Center (GPCC).*

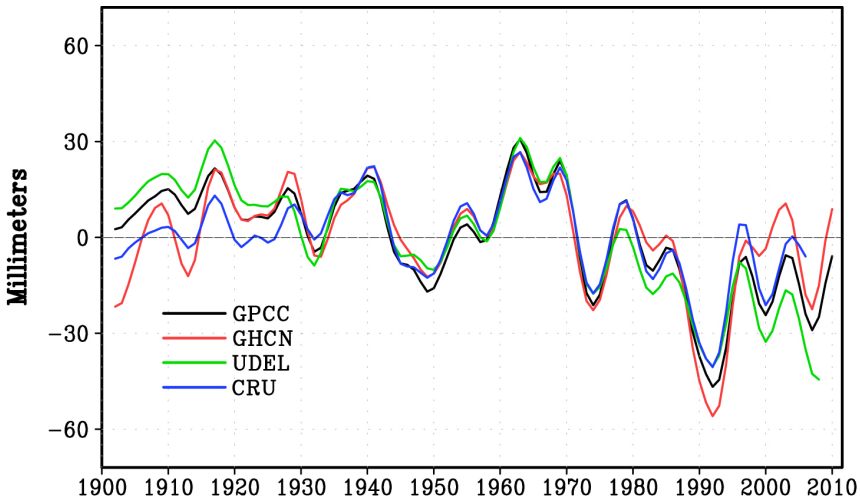

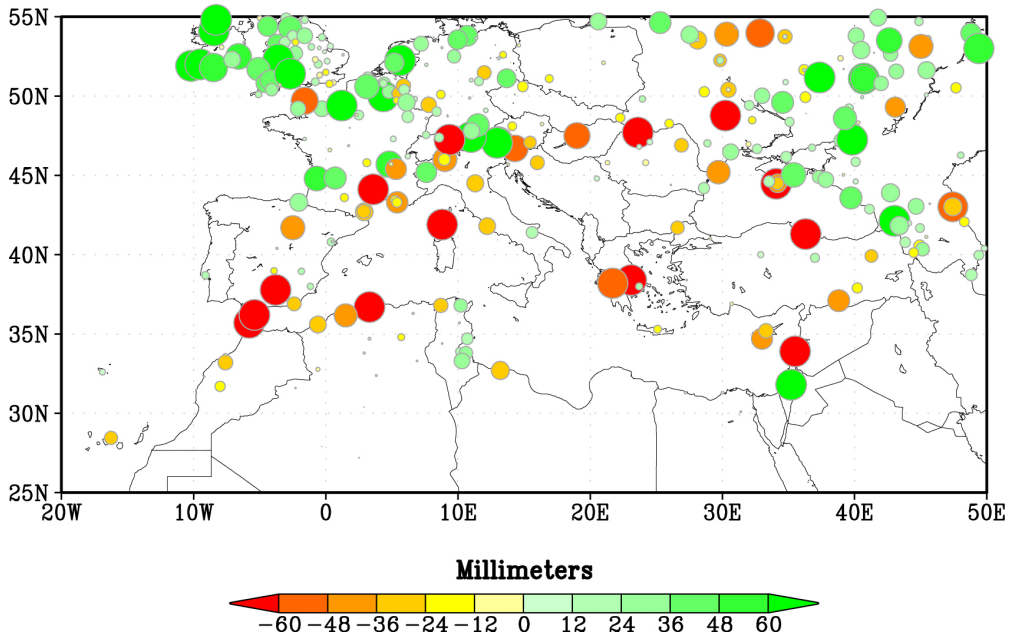

Figure 2. *Time series of Mediterranean (30N-45N; 10W-40E) cold season (Nov-Apr) precipitation for the period 1902-2010 (top) for four observed data sets: GPCC (Global Precipitation Climatology Center), GHCN (Global Historical Climatology Network), UDEL (University of Delaware), CRU (Climatic Research Unit). Anomalies (mm) are referenced to the 1902-2010 period and are smoothed with a 9-pt Gaussian filter. The bottom panel shows a station-based analysis of the change in cold season precipitation for the period 1971-2010 minus 1902-1970; stations are extracted from the GHCN (monthly) and GHCN-d (daily) datasets.*

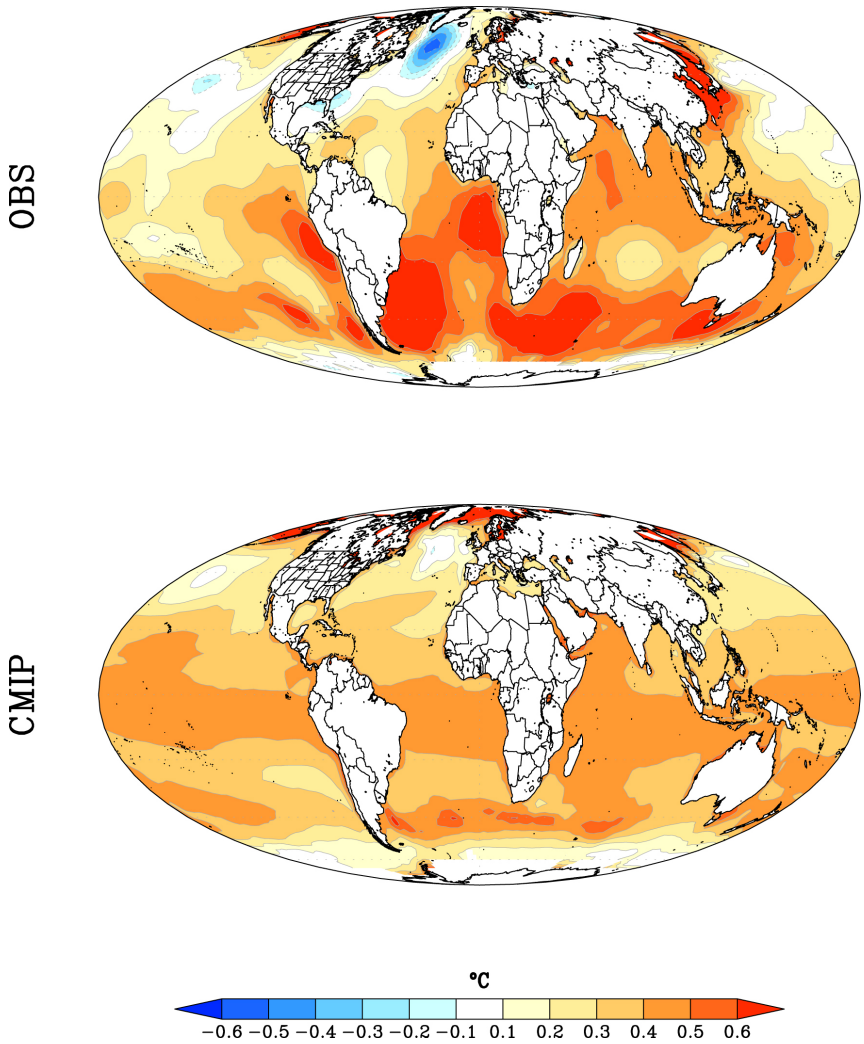

Figure 3. *Cold season (Nov-Apr) sea surface temperature departures (°C) for the period 1971-2010 minus 1902-1970. Top panel: observed analysis from the NOAA merged gridded data set. Bottom panel: Multi-model CMIP3 ensemble sea surface temperatures based on 22 IPCC models.*

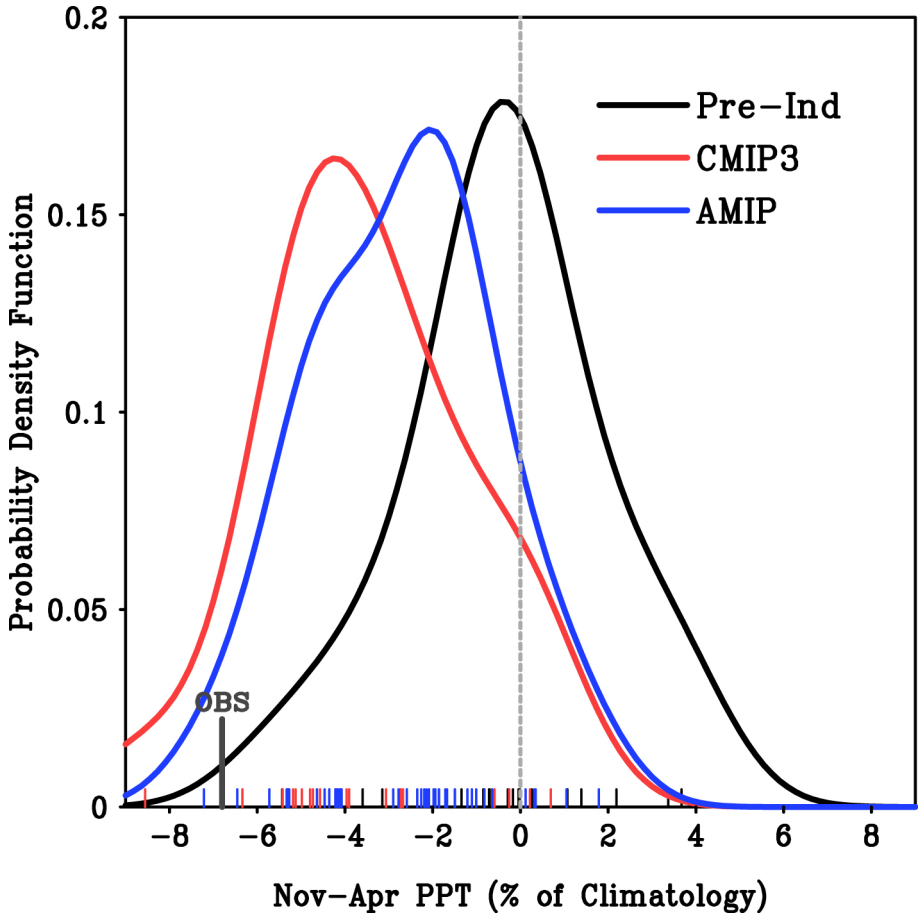

Figure 4*. Probability distribution functions (PDFs) for the 1971-2010 minus 1902-1970 period anomalies of cold season precipitation over the Mediterranean region as % of climatology. The red curve is based on the analysis of 22 IPCC models, while the blue curve is based on 40 AMIP simulations of the 20th century. The solid black curve is drawn from the analysis of 109-yr long samples of unforced integrations from 19 IPCC simulations using pre-industrial concentrations of greenhouse gases. The observed precipitation index decline, based on the average of four analyses (-6.8%) is shown by the gray tick mark to the left. Colored tick marks indicate individual ensemble members.*

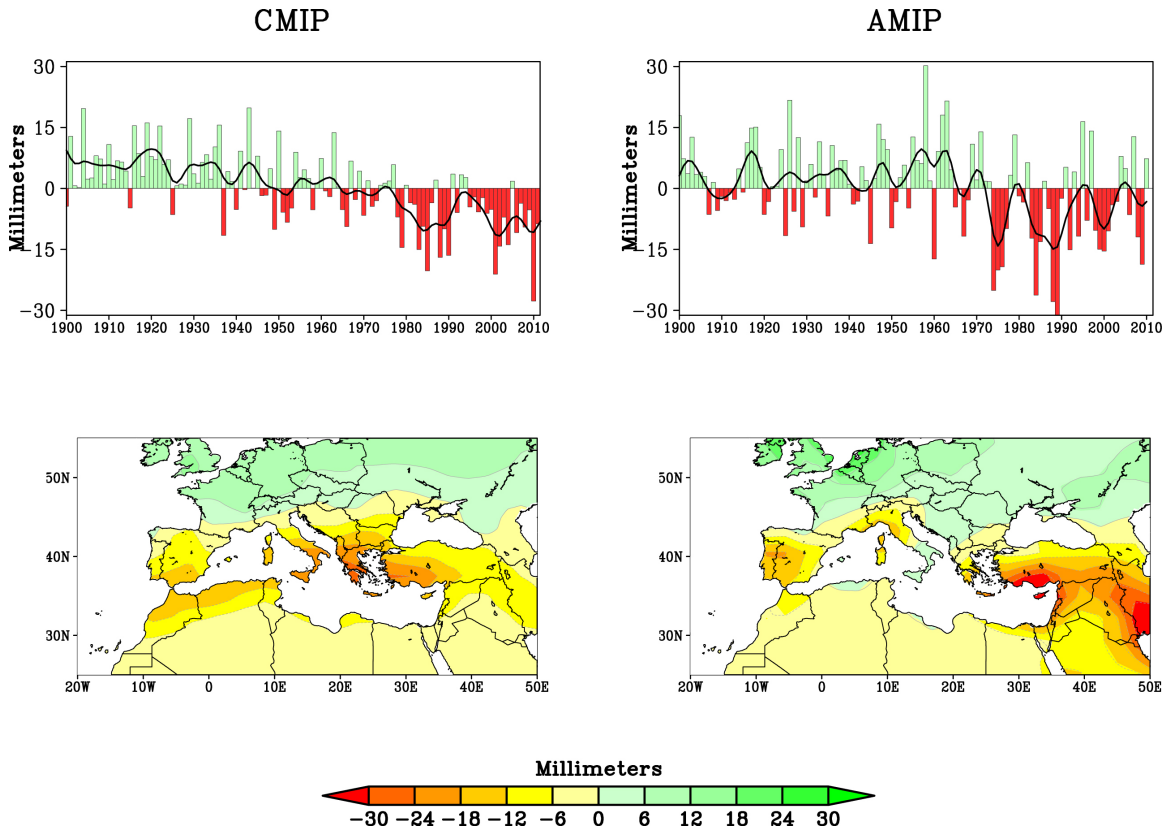

Figure 5. *Simulated change in cold season precipitation (mm) over the Mediterranean region as in Figure 1 based on the ensemble average of 22 IPCC models (left) and the ensemble average of 40 AMIP 20th century runs (right). The difference plots in the lower panels are for the period 1971-2010 minus 1902-1970.*

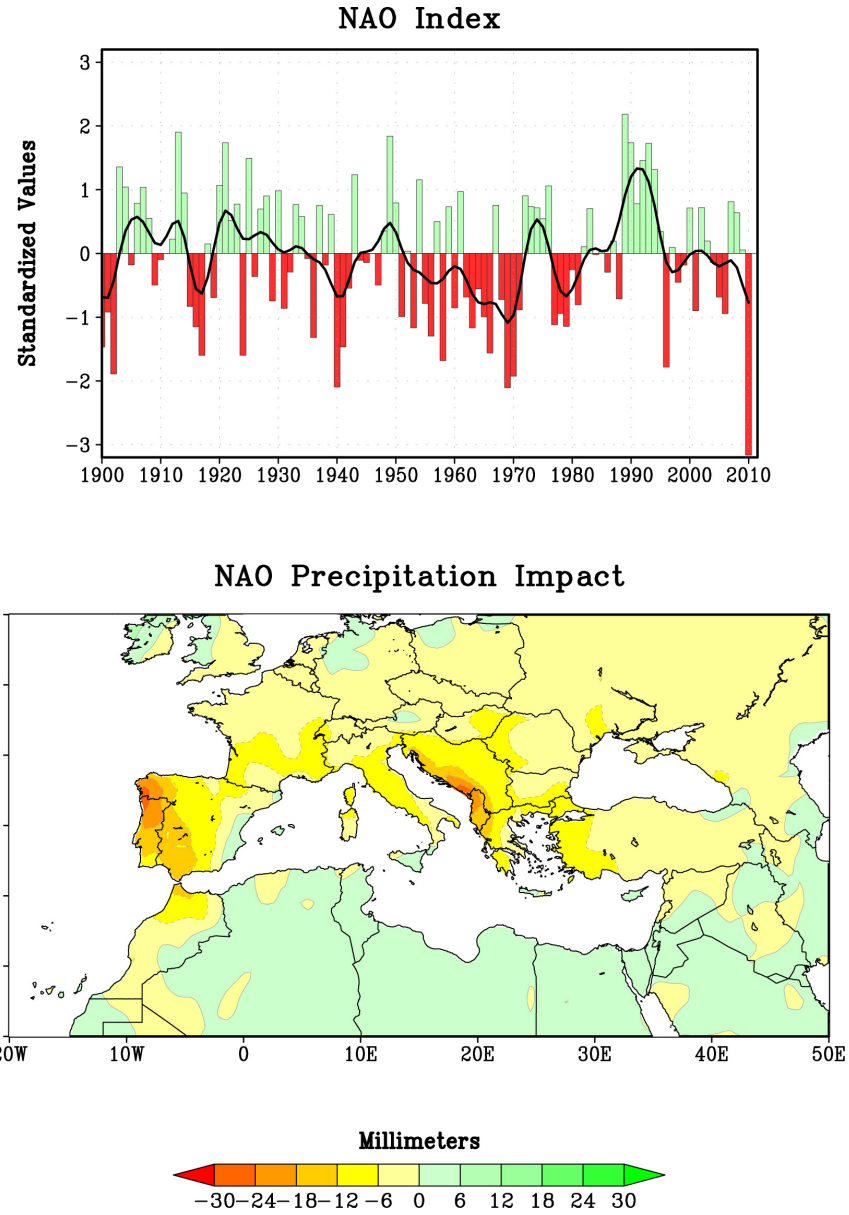

Figure 6. *Time series of an index of the observed North Atlantic Oscillation (NAO) during the cold season (Nov-Apr) for the period 1902-2010 (top) and the change in cold season precipitation for the period 1971-2010 minus 1902-1970 that is linearly related to the change in the NAO index (bottom). NAO index is the principal component time series of the leading empirical orthogonal function of monthly 500 hPa heights during Nov-April over the region 20°N-90°N, 120°W-60°E. Data is the 20th Century Reanalysis, and solid curve is the smoothed NAO time series using a 9-pt Gaussian filter. The precipitation impact (mm) of the NAO change is derived by regressing Nov-Apr precipitation onto the NAO index, and then scaling by the mean difference of the NAO index between the two periods (+0.2 standardized units).*

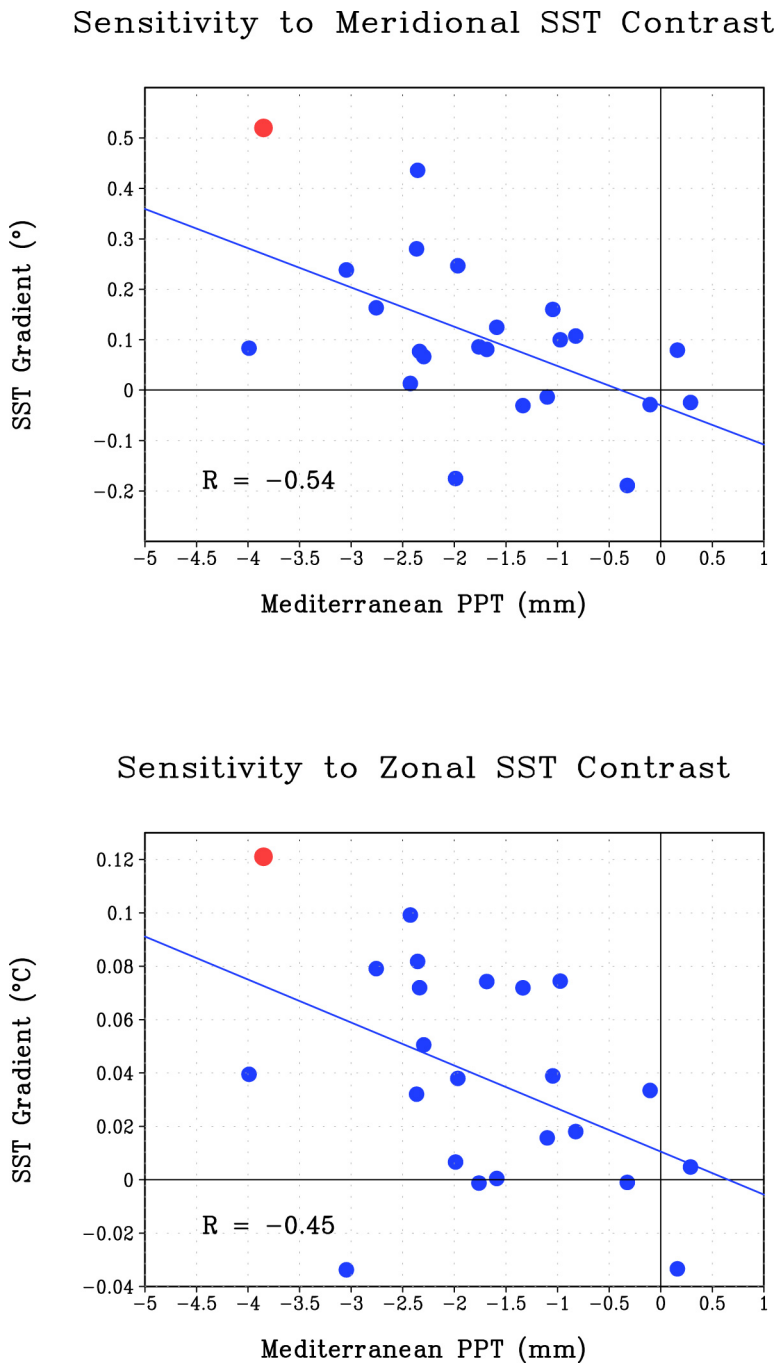

Figure 7. *Relationship between the change (1971-2010 minus 1902-1970) in cold season Mediterranean precipitation (mm) and sea surface temperatures gradient (°C) for the 22 IPCC models. Top panel: Area averaged precipitation versus the meridional (30N-60N minus 30S-30N) SST gradient. Bottom panel: As above but for the zonal (tropical Indian ocean minus tropical Pacific) zonal SST gradient. In both panels the observed value is indicated by the solid red dot.*

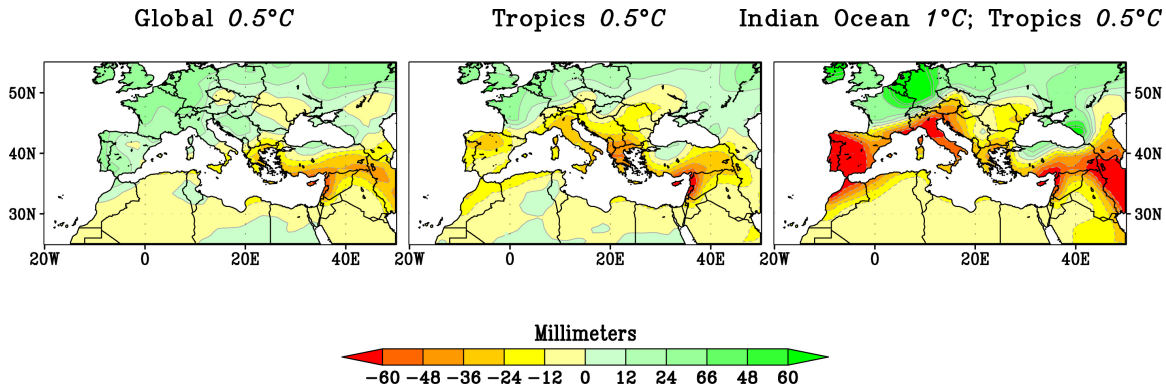

Figure 8. *Forced response of cold season (Nov-April) precipitation(mm) to three SST scenarios. The forced response is the average of 30 simulations using each of three scenarios of changes in SST's: left, uniform warming of +0.5C; middle, warming of +0.5C in the tropics only; right, warming of +1C over the Indian Ocean with +0.5C warming elsewhere in the tropics.*

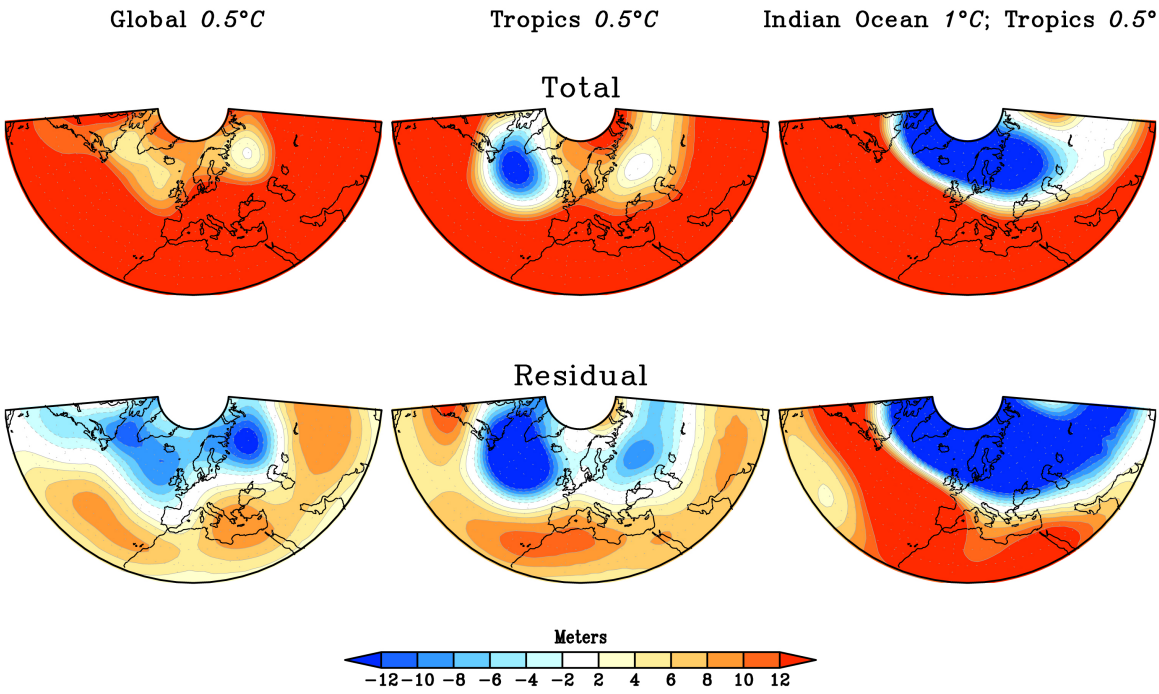

Figure 9. *As in Figure 8 but for the forced response of 500 hPa heights (gpm) to the three SST scenarios. The top panel shows the total height anomaly while the bottom panel shows the residual (global mean removed) height anomaly.*

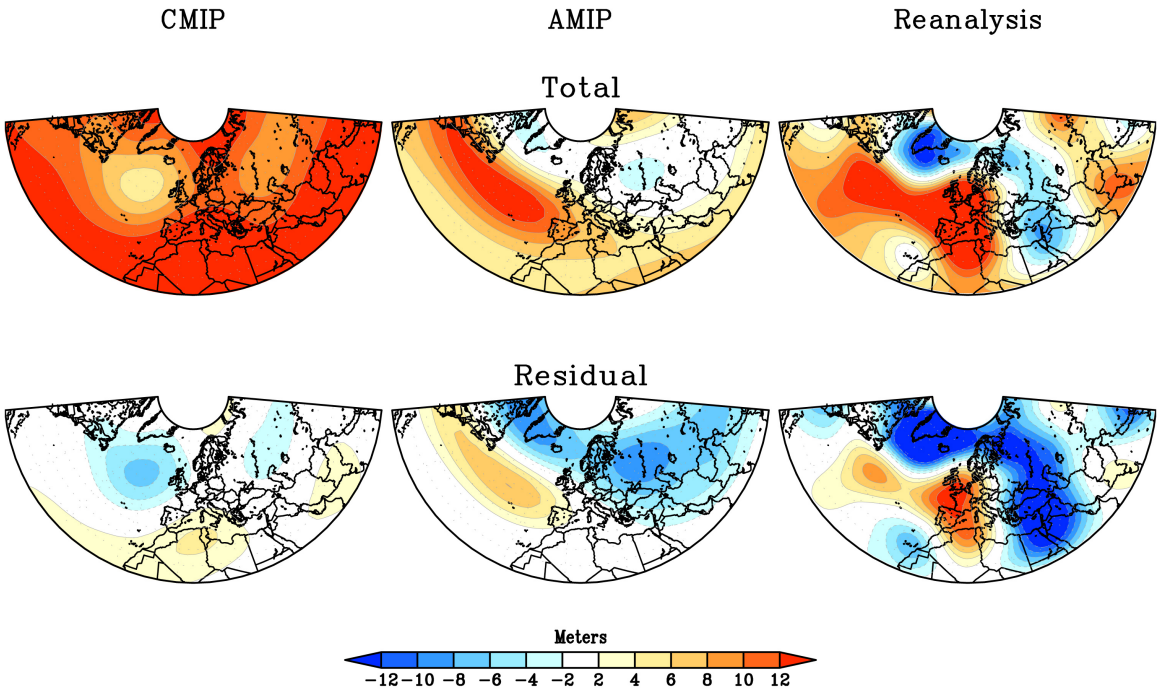

Figure 10. *Cold season (Nov-April) 500 hPa height departures (gpm) for the period 1971-2010 minus 1902-1970 for the 22 model IPCC ensemble average (left), the 40 run ensemble average of 20th century AMIP runs (middle), and based on 20th Century Reanalysis (right). Total height changes are shown in the top panels and the residual fields (with global mean height anomaly removed) below.*